Carbon dioxide sequestration of fly ash alkaline based mortars with recycled aggregates and different sodium hydroxide concentrations: properties, durability, carbon footprint, and cost analysis

14

Mohammad Mastali [1], *Zahra Abdollahnejad* [1], *Fernando Pacheco-Torgal* [1,2]
[1]University of Minho, Guimarães, Portugal; [2]University of Sungkyunkwan, Suwon, Republic of Korea

14.1 Introduction

Carbon dioxide sequestration is crucial for limiting global warming. Several authors (Jang and Lee, 2016) have already studied the possibility of carbon sequestration in ordinary Portland cement (OPC)-based cementitious construction materials, but no CO_2 sequestration studies were performed using alkali-activated materials. These materials are produced though the reaction of an aluminosilicate powder (precursor) with an alkaline activator, usually composed by hydroxide, silicate, carbonate, or sulfate leading to the formation of an amorphous aluminosilicate gel and secondary nanocrystalline zeolite-like structures (Provis, 2014) and have a particular ability for the reuse of several types of wastes (Bernal et al., 2016). Some wastes like fly ash (FA) deserve a special attention because they are generated in high amount and have a very low reuse rate. USA has a reuse rate for FA of around 50% meaning that 30 million tons of FA are not reused annually. Waste glass is also a waste that is generated in relevant quantities and that merits increased recycling efforts. The use of waste glass in alkali-activated binders is especially interesting because its high SiO_2 content allows for a reduction in the content of sodium silicate thus reducing the cost of this binder which constitutes one of the shortcomings of alkali-activated materials (Pacheco-Torgal et al., 2016). This justified recent studies on alkali-activated materials containing waste glass (Martinez-Lopez and Escalante-Garcia, 2016; Wang et al., 2016). This chapter presents results of an investigation concerning carbon dioxide sequestration on FA/waste glass alkaline-based mortars with recycled aggregates and different sodium hydroxide concentrations.

Carbon Dioxide Sequestration in Cementitious Construction Materials
https://doi.org/10.1016/B978-0-08-102444-7.00014-9

14.2 Experimental program

14.2.1 Materials

The mortars were made of FA, calcium hydroxide, waste glass, OPC, recycled aggregates, and a sodium hydroxide solution. The FA was obtained from the PEGO Thermal Power Plant in Portugal and categorized as class B and group N according to the ASTM C618-15. Table 14.1 presents the major oxides of FA particles. The Portland cement is of type I class 42.5 R from SECIL, its composition contains 63.3% CaO, 21.4%SiO_2, 4.0%Fe_2O, 3.3%Al_2O_3, 2.4%MgO, and other minor components. The calcium hydroxide was supplied by LUSICAL H100 and contains more that 99% CaO. Waste glass from glass bottles ground for 1 hour in a ball mill was also used. The final density of the milled waste glass was 1.27 g/cm^3. Solid sodium hydroxide was supplied by ERCROS, S.A., Spain, and was used to prepare the NaOH solution with three different concentrations 7, 8, and 9M. Distilled water was used to dissolve the sodium hydroxide flakes to avoid the effect of unknown contaminants in the mixing water. The NaOH mix was made 24 h prior to use in order to have a homogenous solution at room temperature. A recycled sand to binder ratio of 4 was used in all the mixtures. The recycled sand was obtained from the crushing of concrete blocks and sieving them. The average compressive strength of concrete blocks was around 40 MPa. A sieving operation was carried out to remove dust particles. It was dried at 105°C for 24 h and it was sieved in advance before being used. The dimensions of the sieves were 4.75 and 0.6 mm. The recycled sand had a fineness modulus of 3.885. The detailed grain size distribution of the recycled sand is presented in Fig. 14.1. The recycled sand had a water absorption capacity of 13%. Before use, the recycled sand was carbonated in a carbon chamber from Aralab, model Fitoclima S600 (4.2% CO_2, 40% RH, and 20°C) for 48 h. The recycled sand had a water absorption capacity of 25%. The explanation for the increase of the water absorption relates to the fact that when CSH carbonates, its Ca/Si ratio drops and it becomes highly porous. Studies by NMR spectroscopy indicate that decomposition of C-S-H caused by carbonation involves two steps: (1) a gradual decalcification of the C-S-H, where calcium is removed from the interlayer and defect sites in the silicate chains until Ca/Si = 0.67 is reached, ideally corresponding to infinite silicate chains; (2) calcium from the principal layers is consumed, resulting in the final decomposition of the C-S-H and the formation of an amorphous silica phase (Šavija and Luković, 2016).

Table 14.1 Chemical composition of major oxides in fly ash (FA)

Material	Oxides (wt%)							
	SiO_2	Al_2O_3	Fe_2O_3	CaO	MgO	Na_2O	K_2O	TiO_2
FA	60.81	22.68	7.64	1.01	2.24	1.45	2.7	1.46

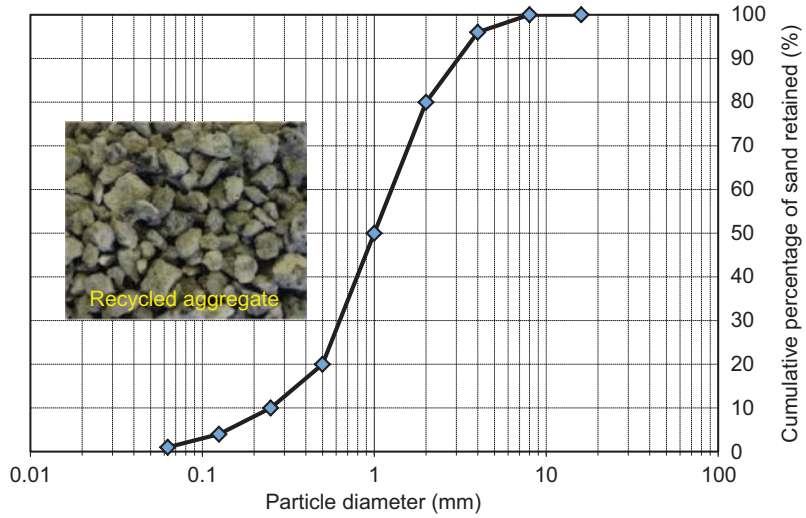

Figure 14.1 Distribution of sand particles.

14.2.2 Mix design and mortar production

The composition of the mortars is shown in Table 14.2. In the batching process of the mortars, dry ingredients (FA, recycled sand, calcium hydroxide (or cement), metakaolin, and milled glass) were mixed for 2 min. Then, sodium hydroxide was added and again mixed for 3 min. Then, the mixed mortars were cast into cubic molds ($50 \times 50 \times 50\ mm^3$) to assess the compressive strength and in prismatic beams with dimension ($40 \times 40 \times 160$ mm) to assess the flexural strength. The specimens were cured for 24 h at lab conditions (averagely 25°C and 40% RH) and then they were demolded. Then the specimens were cured in the carbonation chamber (4.2% CO_2 concentration and 40% RH) for 7 days and in the lab conditions for the remaining days until the age of the test. This is because preliminary experiments showed that all mixtures were fully carbonated during 7 days through a CO_2 preconditioning curing. Three specimens with dimension of $50 \times 50 \times 50\ mm^3$ were cast and used to measure the CO_2 sequestration by using a furnace decomposition method (El-Hassan and Shao, 2015). The carbonated specimens were placed initially in the oven at 105°C for 24 h to evaporate any absorbed water. Then, the weights of the dried specimens were recorded. Afterwards, the specimens were put in the calciner at a temperature between 500 and 850°C for 4 h to measure the water bound to hydration products and carbon dioxide in carbonates. The results revealed that 800°C could be used as the appropriate decomposition temperature.

Table 14.2 Proportions of mix compositions (kg/m^3)

Mixtures	Fly ash	CH	PC	MK	MG	SH	Sand	Molarity (mol/L)
80FA_10CH_10 MG_RAGC_CC_7M	340.0	42.5	–	–	42.5	215.5	1700.0	7
80FA_10 PC_10 MG_RAGC_CC_7M	341.0	–	43.0	–	43.0	213.0	1706.0	
80FA_10CH_10 MG_RAGC_CC_8M	340.0	42.5	–	–	42.5	215.5	1700.0	8
80FA_10 PC_10 MG_RAGC_CC_8M	341.0	–	43.0	–	43.0	213.0	1706.0	
80FA_10CH_10 MG_RAGC_CC_9M	340.0	42.5	–	–	42.5	215.5	1700.0	9
80FA_10 PC_10 MG_RAGC_CC_9M	341.0	–	43.0	–	43.0	213.0	1706.0	

CH, calcium hydroxide; *FA*, fly ash; *MG*, waste glass; *PC*, Portland cement; *SH*, sodium hydroxide.

14.2.3 Test procedures

14.2.3.1 Compressive strength

The compressive strengths of the mixtures were assessed at different ages of 7, 14, and 28 days. The compressive strength of each mixture was obtained by averaging the replicated three cubes. All cubic specimens were assessed under compressive load with a constant displacement rate of 0.30 N/mm^2 s, as per the ASTM C109 recommendation. The compressive load was measured with a load cell of 200 kN capacity.

14.2.3.2 Flexural strength

Flexural performance was assessed under Three Point Bending (TPB) load conditions, as indicated in Fig. 14.2. The flexural load was applied to the beams with a displacement rate of 0.6 mm/min. The flexural load was measured with a load cell of 50 kN capacity. Eq. (14.1) was used to calculate the flexural strength of specimens under TPB test:

$$\sigma_f = \frac{3FL}{2bh^2} \tag{14.1}$$

where, F is the total flexural load, L is span length, b and h are width (40 mm) and height (40 mm) of beams, respectively.

14.2.3.3 Water absorption

The water absorption by immersion method was based on three cubic specimens with a 100 mm edge per mixture. The specimens with age of 28 days were dried

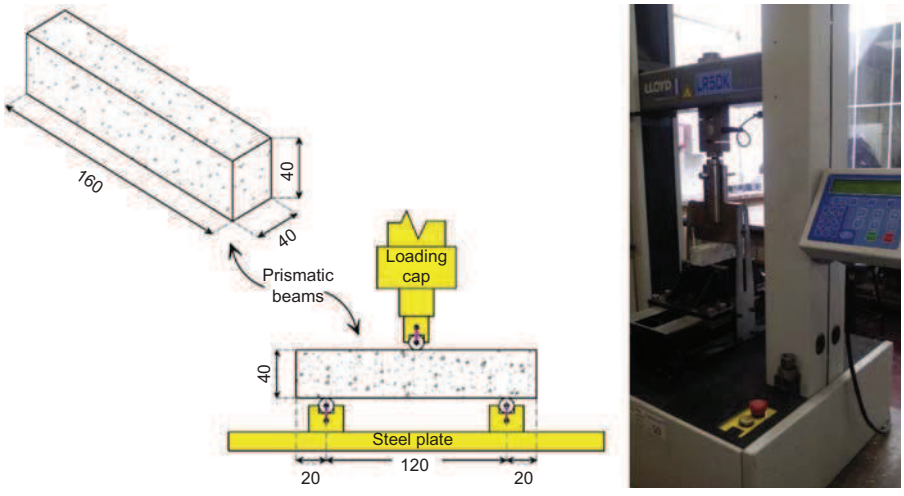

Figure 14.2 Adopted test setup for implementation of the flexural test.

at the temperature of 105°C.The specimens were then immersed in the water container at 23±2°C until saturation of the specimens. Next, the specimens were submerged in water using a mesh container and the mass of the submerged specimen has been recorded as immersed mass (*Wim*). Then, the specimens were removed from the last position and the surface of the specimen was cleaned using a wet cloth and immediately the weight of the specimens were measured as W_{sat}. Then, the specimens were heated in a standard oven at 105°C until they were dry (reaching a constant mass) and the dried mass of the specimens was noted as W_{dry}. Absorption coefficient (A%) was determined for all the specimens using (Eq. 14.2):

$$\mathrm{A}(\%) = \frac{W_{sat} - W_{dry}}{W_{sat} - W_{im}} \times 100 \tag{14.2}$$

The water absorption by capillary method was performed based on the EN 1015-18 standard using three cubic specimens with a 100 mm edge per mixture. Prior to water absorption by capillary method, the surface area of the specimens were coated with silicon (except for failure surface resulted from flexural test) in order to assure the water can be absorbed from one surface of the specimens that is soaked in water. The quantification of absorbed water was performed by conducting weighings of the specimens at several segment intervals which started at 0, 5, 10, 20, 30, 60, 90, 120, 180, 240, 300, 360,1440, and 2880 min. However, it should be mentioned that, in order to assess the evolution of the water absorption toward weight stabilization, periodic measurements were performed for about 4 days. The capillary absorption coefficient was determined using (Eq. 14.3):

$$C = \frac{M2 - M1}{\sqrt{tf - ti}} \tag{14.3}$$

in which, C is the capillary absorption coefficient (kg/(m^2 min$^{0.5}$)); $M2$ is the weight if the specimen in contact with water at the instant 90 min (kg/m^2); $M1$ is the weight if the specimen in contact with water at the instant of 10 min (kg/m^2); tf is the final time, instant of 90 min (min); and ti is the initial time, instant of 10 min (min).

14.2.3.4 Elastic modulus

According to the ASTM C469 recommendation, three cylinders with 50-mm diameter and 100-mm height were submitted by the compressive loading to define the elastic modulus of the different mixtures. The apparatus consisted of two aluminum rings with screws for attachment to the specimen and three Linear Variable Differential Transformer (LVDT) of 50-mm stroke used to record displacements around the cylinders, as shown in Fig. 14.3. To obtain the elastic modulus, the specimens were subjected to a cyclic compressive load up to 40% the compressive strength.

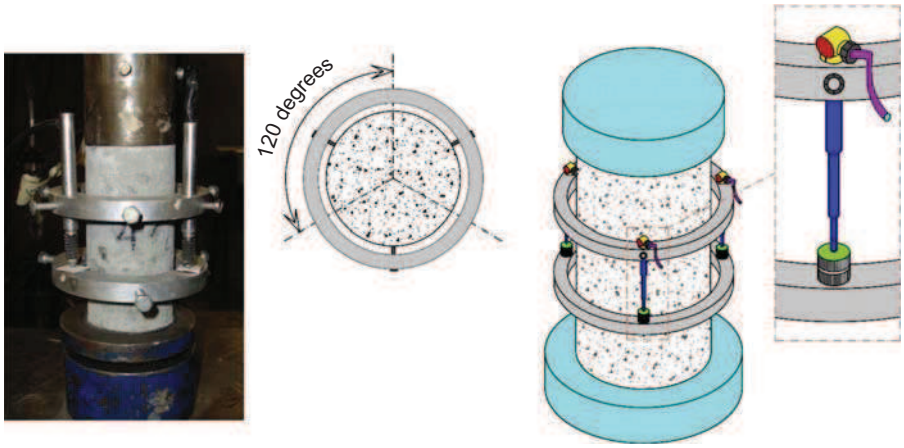

Figure 14.3 The test set-up used to assess the elastic modulus of the mixtures.

14.2.3.5 Drying shrinkage

With respect to the ASTM C596-09 recommendation, three prismatic beams with dimension 25 × 25 × 305 mm were cast and prepared for each mixture to assess the rate of drying shrinkage. After demolding, the beams were cured in a carbonation chamber using flow-through CO_2 gas. In the present study, Graff-Kaufman method was employed to record the length variations of prismatic beams after demolding. Employing this method eliminates early registration of length changes. The apparatus used to measure the length variation is indicated in Fig. 14.4. Two steel snails were installed at both end sides of the beams to measure length changes of specimens. An installed steel snail was mounted on a fixed steel base and the other steel snail (for the other side) was installed in a digital gauge with the accuracy of 0.001 mm, as shown in Fig. 14.4. The drying shrinkage rates for the mixtures were measured for more than 40 days. Stabilization of the length variations was taken into account as the main criterion to stop the shrinkage test.

14.2.3.6 Freeze/thaw resistance

To assess freeze/thaw resistance, three cubic specimens with dimension 100 × 100 × 100 mm were cast and tested after 28 days using compressive test. The equipment to test freeze-thaw resistance, Model Fitoclima 1000, is shown in Fig. 14.5. The freeze-thaw test was carried out according to PD CEN/TS 12390-9: 2016 standard with temperatures ranging from −18 to +20°C. The specimens were kept for 13 h in −18°C and 3 h in +20°C. The transitions from positive to negative and negative to positive temperatures took 3 and 5 h, respectively. Fig. 14.6 shows a freeze-thaw cycle. The specimens were subjected to 50 cycles.

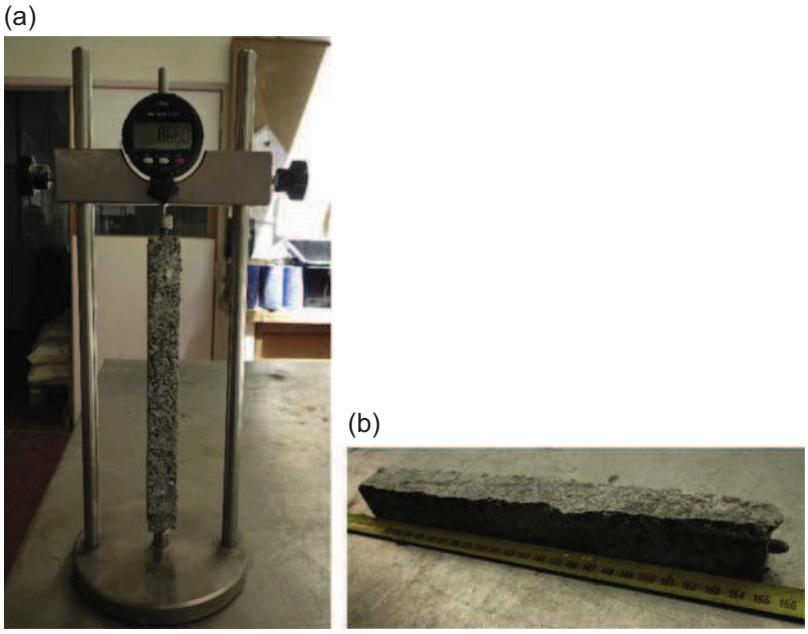

Figure 14.4 (a) The apparatus used to measure the length changes; (b) the prismatic beams used to assess the rate of drying shrinkage.

Figure 14.5 Equipment for testing freeze-thaw resistance.

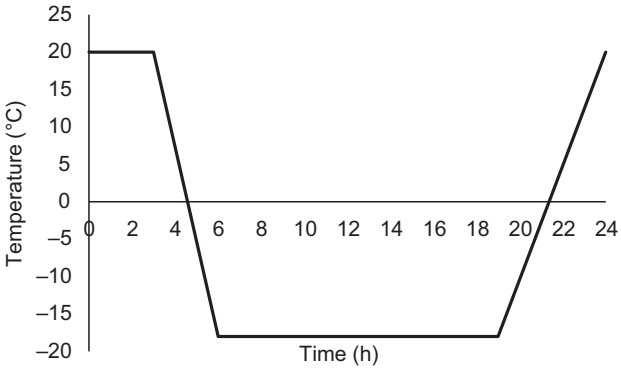

Figure 14.6 Temperature variation for one freeze/thaw cycle.

14.3 Results and discussion

14.3.1 Compressive strength

Fig. 14.7 shows the compressive strength of different mixtures. Regardless of the mixture type and curing age, increasing the molarity from 7 to 8 M increased the compressive strength. The maximum increase of the compressive strength was measured in the mixture 80FA_10CH_10 MG_RAGC_CC_8M with about 60%, as compared to 80FA_10CH_10 MG_RAGC_CC_7M. Several authors already reported that a high concentration of sodium hydroxide leads to an increase in the coagulation of silica and a reduction in the compressive strength (Rattanasak and Chindaprasirt, 2009; Gorhan and Kurklu, 2014; Atis et al., 2015). In general the replacement of Portland cement by calcium hydroxide is associated with an increase in the compressive strength. The explanation could be associated to the fact that the replacement may lead to the formation of a higher amount of CSH gel. This is because of the low sodium hydroxide concentration used in the present study (Garcia-Lodeiro et al., 2016) that favors CSH formation. Thus no consistent trend for the compressive strength was found due to increase in the molarity from 8 to 9M. For instance, the compressive strength increased around 30% for the mixture 80FA_10 PC_10 MG_RAGC_CC at the age of 7 days by increasing the molarity from 8 to 9M, while the compressive strength decreased by about 15% for the mixture 80FA_10CH_10 MG_RAGC_CC. The explanation for the compressive strength loss with high sodium hydroxide concentration from 8 to 9M is not related to an increase in leaching of silica and alumina from FA as reported by some scientists (Sata et al., 2013; Hanjitsuwan et al., 2014) because that explanation is only valid for sodium hydroxide concentrations above 10M that lead to the formation of aluminosilicate species (Alonso and Palomo, 2001a,b). Increasing the duration of curing also increased the compressive strength, so that the maximum compressive strength for the specimens at the age of 14 days was measured around 9 MPa in the mixture 80FA_10CH_10 MG_RAGC_CC_8M.

Furthermore, no variation in the compressive strength of mixtures was detected by increasing the curing duration from 14 to 28 days. The maximum compressive strength was found around 10 MPa in the mixture 80FA_10CH_10 MG_RAGC_CC_8M. Interestingly, it was found that the maximum compressive strength at the early age (7 days for the mixture of 80FA_10CH_10 MG_RAGC_CC_8M) was about 70% of the compressive strength at the final age (28 days).

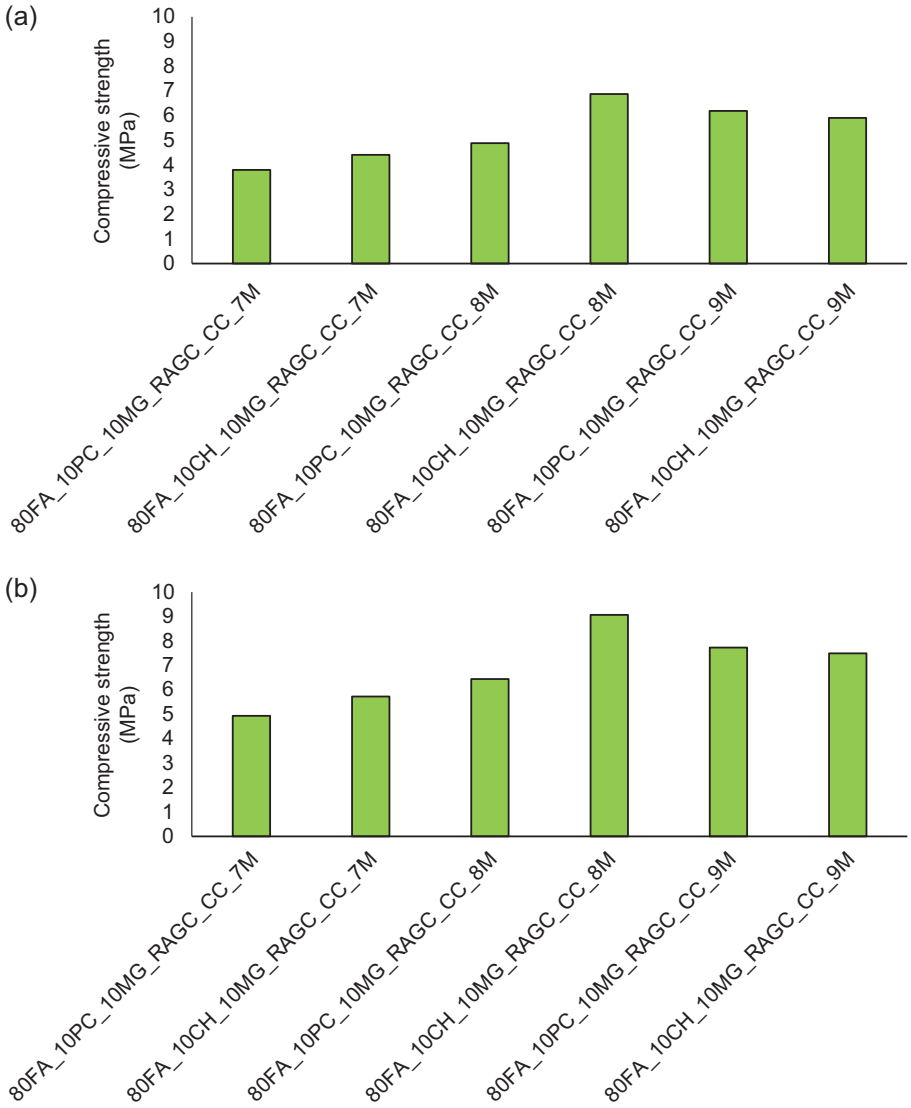

Figure 14.7 The compressive strength of the mixtures cured for: (a) 7 days; (b) 14 days; (c) 28 days.

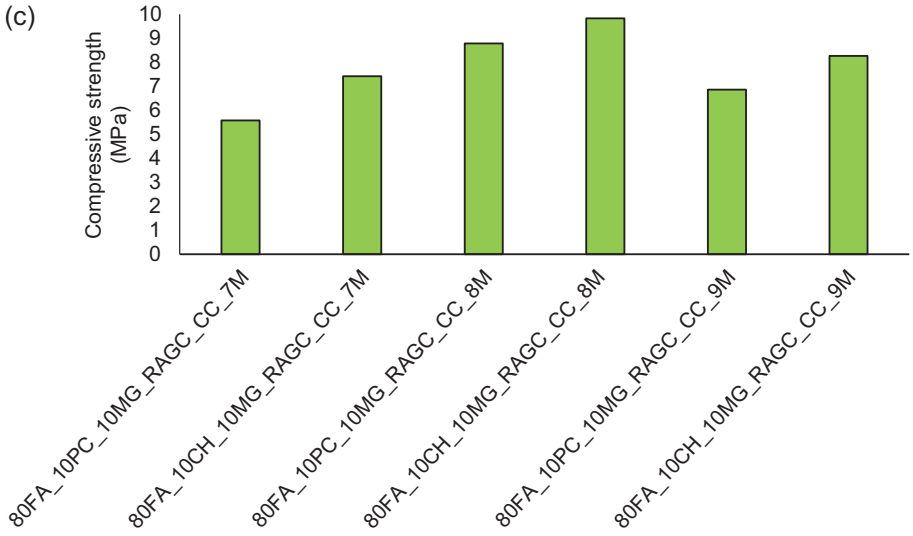

Figure 14.7 cont'd.

14.3.2 Flexural strength

Fig. 14.8 illustrates the results obtained for the flexural strength. Similar to the results obtained for the compressive strength, the maximum flexural strength was detected in the mixture containing sodium hydroxide with the molarity of 8M, so that the maximum flexural strengths around 3.5 and 2.5 MPa were recorded for the mixtures

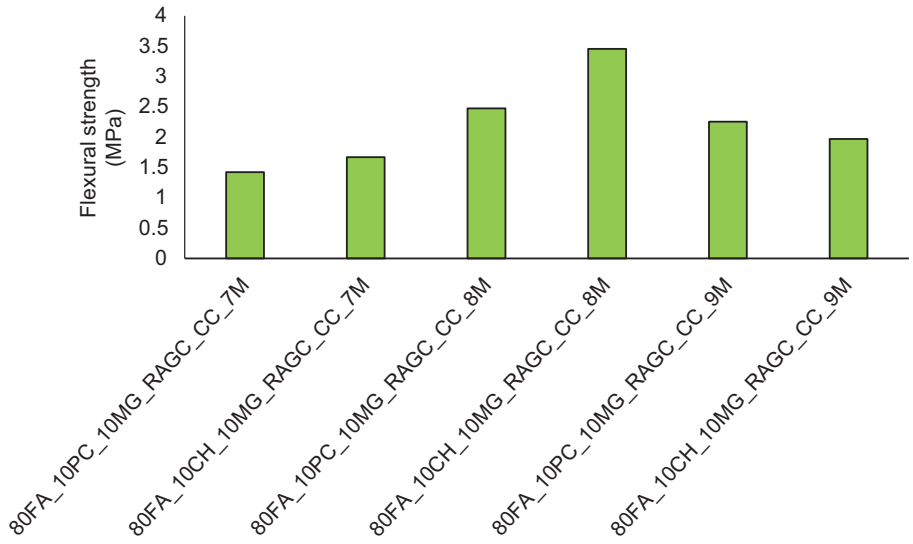

Figure 14.8 Flexural strength.

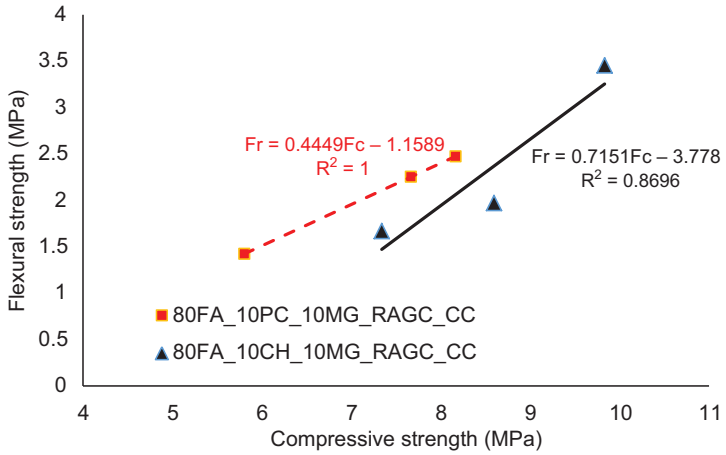

Figure 14.9 Correlation between the compressive strength and the flexural strength.

of 80FA_10CH_10 MG_RAGC_CC_8M and 80FA_10 PC_10 MG_RAGC_CC_8M, respectively. Increasing the molarity from 7 to 8M increased about 75% and 210% the flexural strength of the mixtures 80FA_10CH_10 MG_RAGC_CC and 80FA_10 PC_10 MG_RAGC_CC, respectively, while increasing the molarity from 8 to 9 M reduced about 10% and 45% the flexural strength of the mixtures 80FA_10CH_10 MG_RAGC_CC and 80FA_10 PC_10 MG_RAGC_CC, respectively. Fig. 14.9 shows the correlation between the flexural strength and the compressive strength of the mixtures, consisting high coefficient of determination. F_r represents the flexural strength. With respect to the developed equations, the rate of improving the mechanical properties of the mixture 80FA_10CH_10 MG_RAGC_CC was higher when compared to the mixture 80FA_10 PC_10 MG_RAGC_CC.

14.3.3 Water absorption

Fig. 14.10 depicts the results of water absorption by immersion and density. The minimum water absorption of around 9.4% is noticed for the mixtures with a sodium hydroxide concentration of 8M, the ones that were associated to a higher compressive strength. No relevant differences were noticed when calcium hydroxide was replaced by Portland cement. An increase in the sodium hydroxide concentration from 7 to 8M lead to a water absorption reduction of 5% and 10% for the mixtures based on OPC and calcium hydroxide, respectively. As to the reduction from 8 to 9M a minor water absorption increase was noticed of 5% and 3% for the mixtures based on OPC and calcium hydroxide, respectively. The minimum and maximum density were recorded in the mixture consisting of sodium hydroxide with concentrations of 7M (80FA_10 PC_10 MG_ RAGC_CC_7M with density of 2172 kg/m^3 and 80FA_10CH_10 MG_RAGC_CC_7M with density of 2144 kg/m^3) and 8M (80FA_10 PC_10 MG_RAGC_CC_8M with density of 2210 kg/m^3 and

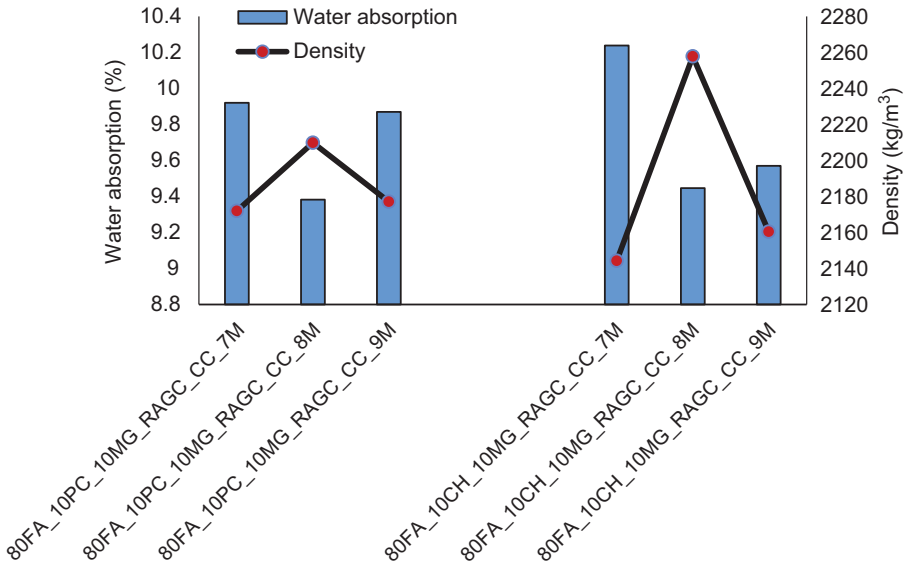

Figure 14.10 Water absorption versus density.

80FA_10CH_10 MG_RAGC_CC_8M with density of 2258 kg/m^3), respectively. Fig. 14.11 depicts the capillary water absorption coefficients. Regardless of the concentration of the sodium hydroxide, replacing calcium hydroxide by OPC is associated to a reduction of the capillary water absorption coefficients. The maximum reduction was measured to be more than 40% in the mixture containing the molarity

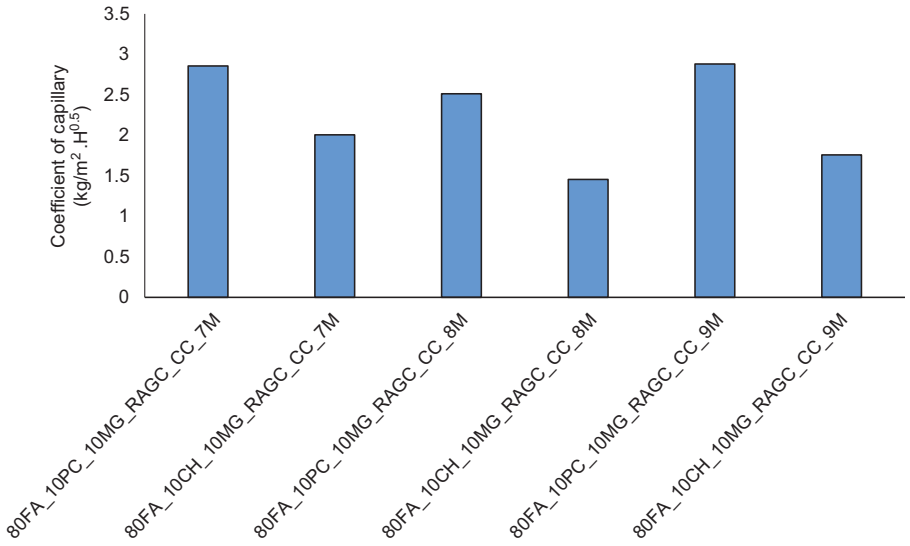

Figure 14.11 Capillary absorption coefficient.

8M. This coefficient was varied in the range of 1.45−2 kg/m^2 H$^{0.5}$ for the mixtures containing calcium hydroxide, while this coefficient was found to be in the range of 2.51−2.88 kg/m^2 H$^{0.5}$ for the mixtures containing OPC. Since the tendency of mixtures to absorb and transmit water by capillary action in the plain mixture functions by the capillary network, porosity, and tortuosity in the matrix, this means that the use of calcium hydroxide is associated to a denser microstructure. Abdollahnejad et al. (2017) also studied alkaline-based mixtures reporting water absorption capillarity coefficients in the range of 2.25−4 kg/m^2 H$^{0.5}$ where a lower OPC content was associated with higher values. Since lower capillarity coefficients were reported in this study for mixtures with minor amount of calcium hydroxide, it is possible that the accelerated carbonation curing has been responsible for a coarser capillarity network.

14.3.4 Elastic modulus

The results of the elastic modulus are shown in Fig. 14.12. Regarding the results, increasing the sodium hydroxide molarity increased the stiffness of the mixtures, so that the maximum elastic modulus was recorded in the mixtures containing sodium hydroxide of concentration 9M. Moreover, it was detected that using calcium hydroxide instead of OPC increased the elastic modulus of the mixtures, regardless of the molarity. Therefore, the maximum elastic modulus was measured around 800 MPa

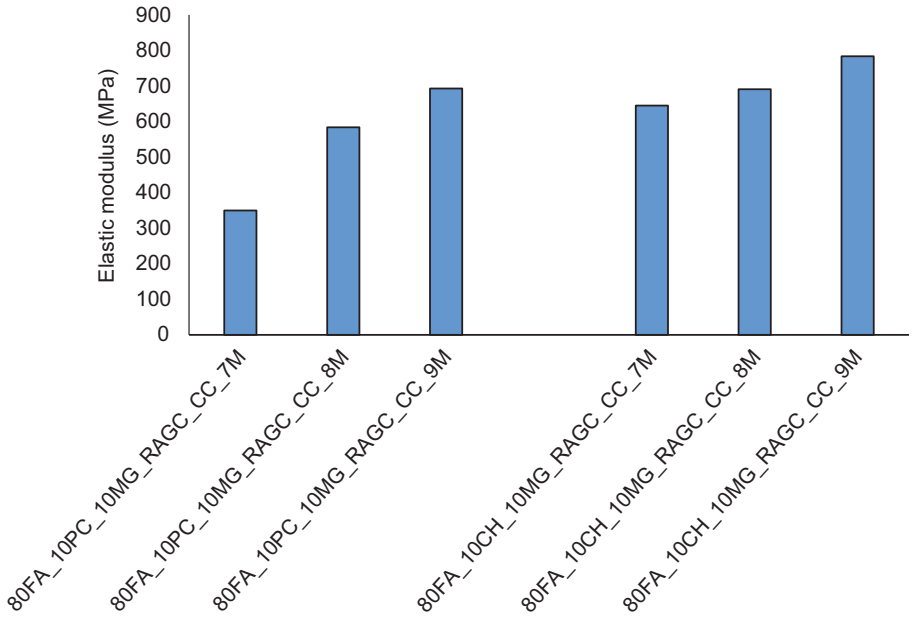

Figure 14.12 Elastic modulus.

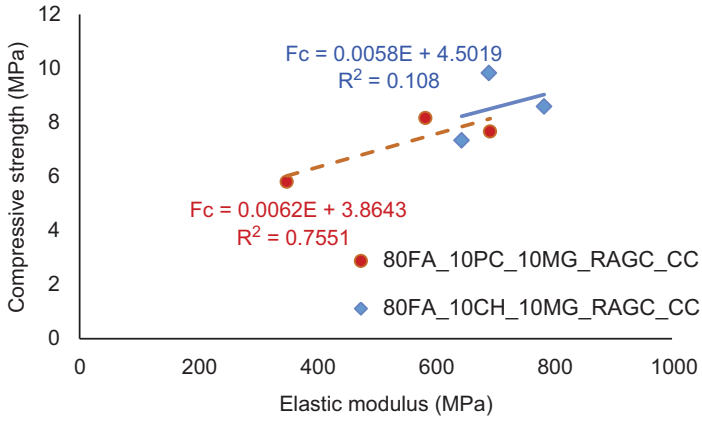

Figure 14.13 Correlation between the compressive strength and elastic modulus.

in the mixture of 80FA_10CH_10 MG_RAGC_CC_9M. For the mixture of 80FA_10 PC_10 MG_RAGC_CC, the maximum increase of the elastic modulus was recorded as 66% due to increase in the molarity from 7 to 8M. Thus for the mixture of 80FA_10CH_10 MG_RAGC_CC, the maximum increase of the elastic modulus achieved was 13% due to increase of the molarity from 8 to 9M, as indicated in Fig. 14.13, where E is the elastic modulus and F_C is the compressive strength. The analytical results from the correlation between elastic modulus and the compressive strength revealed that the elastic modulus increases with the compressive strength with higher rate of OPC in the mixture rather than calcium hydroxide. Also a significant correlation between elastic modulus and compressive strength was found in the mixture based on OPC but not with the mixture based on calcium hydroxide. Moreover, these results were found in the mixture of 80FA_10 PC_10 MG_RAGC_CC rather than the mixture of 80FA_10CH_10 MG_RAGC_CC.

14.3.5 Drying shrinkage

The drying shrinkage results are depicted in Fig. 14.14. Regardless of the mixture and concentration of sodium hydroxide, the rates of drying shrinkages were characterized by higher initial growth, reaching approximately 50% of the total drying shrinkage rate at the first 7 days for the majority of the mixtures. The minimum and maximum rates of drying shrinkage were recorded for the mixtures 80FA_10CH_10 MG_RAGC_CC_8M (0.0131 με) and 80FA_10CH_10 MG_RAGC_CC_9M (0.0231 με), respectively. Moreover, the minimum rate of drying shrinkage for the mixture 80FA_10CH_10 MG_RAGC_CC was measured by sodium hydroxide concentration of 8M. Regardless of the mixture type, the maximum rate of drying shrinkage was recorded in the mixtures containing the molarity of 7M. The results can be partially explained by the results of the modulus of elasticity because mixtures with a lower stiffness have a higher shrinkage. Also these results are in line with the capillary water absorption and can be explained by the fact that finer capillary networks are associated with higher capillary stress that generates shrinkage.

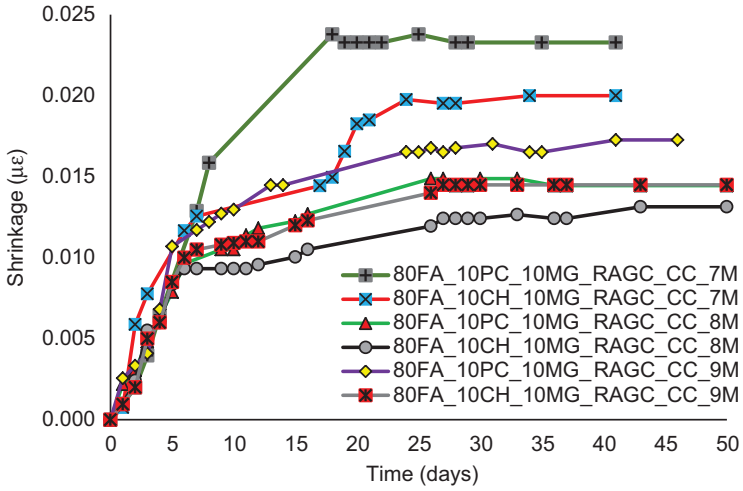

Figure 14.14 Drying shrinkage.

14.3.6 Freeze-thaw resistance

Fig. 14.15(a) shows the results of compressive strength of reference mixtures cured at ambient temperature and the compressive strength after 50 cycles of freeze/thaw. The results show that mixtures based on OPC have lower strength loss than mixtures that are based on calcium hydroxide. The differences in the strength loss depend on pore sizes and distributions, which affect the permeability of the matrix and the distance to the nearest unfilled void. When water freezes in the pores of the matrix, an expansion in the volume of frozen water occurs, forcing the excess water through the boundaries. The magnitude of this hydraulic pressure depends on the permeability of the matrix, the degree of saturation, the distance to the nearest unfilled void, and the rate of freezing, so that this hydraulic pressure exceeds the tensile strength of the matrix forming the cracks. In further freezing cycles, new cracks will be formed and the deterioration will proceed. Fig. 14.15(b) shows the results of mass loss. The results are very similar for the different mixtures, around 1% mass loss, except for the mixture based on OPC and a sodium hydroxide concentration of 8M that has a 2.7% mass loss percentage. The mass loss on the freeze-thaw test for the number of cycles used in this study occurred mostly on the surface of the specimens, thus not helping us to correlate the results with the results of compressive strength.

14.3.7 CO_2 sequestration

Fig. 14.16 depicts the results of CO_2 sequestration. The results show that for mixtures that contain OPC, increasing sodium hydroxide molarities from 7 to 9M consistently increased the amount of the CO_2 sequestration. However, when the mixtures are compared for the same sodium hydroxide concentration that contain no OPC, no differences are detected for both 7M-based mixtures (130 $kgCO_2eq/m^3$) and 9M-based

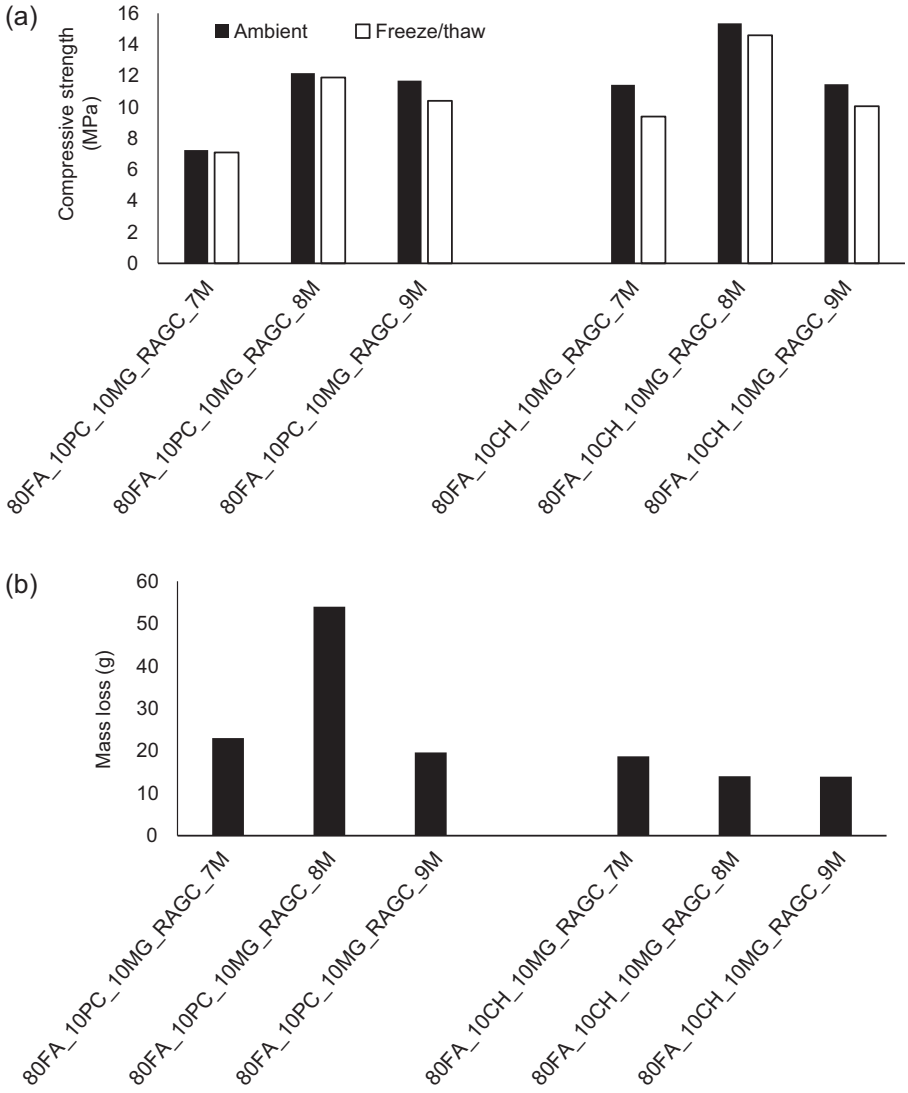

Figure 14.15 Effect of freeze/thaw on: (a) the compressive strength; (b) mass loss.

mixtures (152 $kgCO_2eq/m^3$). For mixtures based on calcium hydroxide the maximum CO_2 sequestration (164 $kgCO_2eq/m^3$) is noticed for the mixture with a sodium hydroxide concentration of 8M. Since the diffusivity of CO_2 in alkali-activated materials is controlled by the same variables as identified in conventional Portland cements, namely the porosity and permeability of the material, and since this mixture does not have a higher water capillary coefficient (which is a proxy of permeability), the higher carbon sequestration capacity of this mixture must be associated to a higher content of CSH that were carbonated. Other authors (El-Hassan and Shao, 2014)

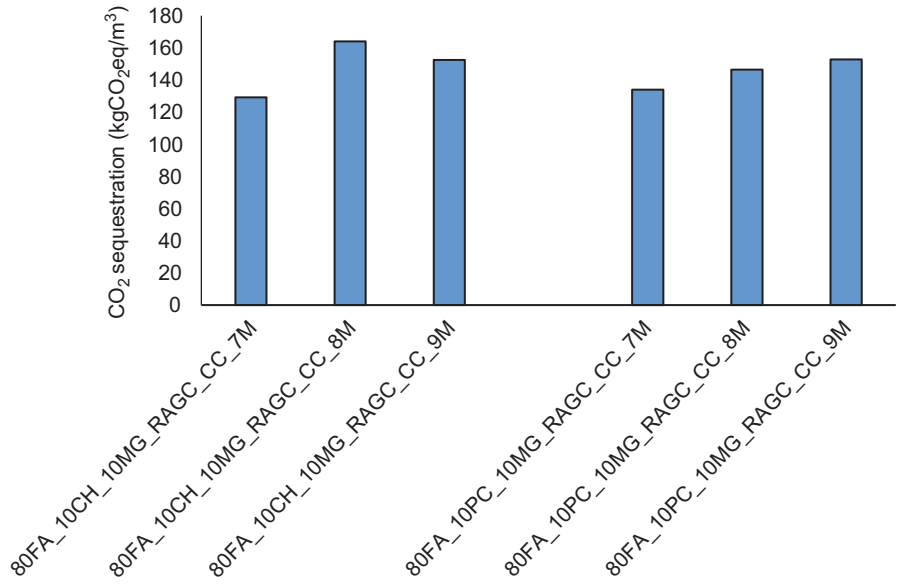

Figure 14.16 CO_2 sequestration.

have studied the CO_2 sequestration using accelerated CO_2 curing in the concrete blocks containing 13% OPC, reporting a sequestration of 75 $kgCO_2eq/m^3$. This means that alkali-activated materials have a higher carbon sequestration capacity.

14.3.8 The carbon footprint

The greenhouse gas (GHG) ($kgCO_2eq/m^3$) results were obtained using the EcoInvent database. Table 14.3 shows the global warming potential for each mortar constituent. The results of GHG emissions as well as the carbon footprint of the mixtures are indicated in Fig. 14.17. The results show that GHG emissions are strongly dependent on the increase of the sodium hydroxide concentration. This is because this component has a high global warming potential. The results also show that the mixtures with the additive OPC have higher GHG emissions. As a consequence the highest GHG emissions (175 $kgCO_2eq/m^3$.) are noticed for OPC mixtures with a sodium hydroxide concentration of 9M, while the lowest (132 $kgCO_2eq/m^3$) is associated with the

Table 14.3 Global warming potential of each component of mixture ($kgCO_2eq$)

Recycled aggregates	MG	CH	Fly ash	Water	PC	SH
0.00401	0.00526	0.416	0.00526	0.000155	0.931	2.24

CH, calcium hydroxide; *FA*, fly ash; *MG*, waste glass; *PC*, Portland cement; *SH*, sodium hydroxide.

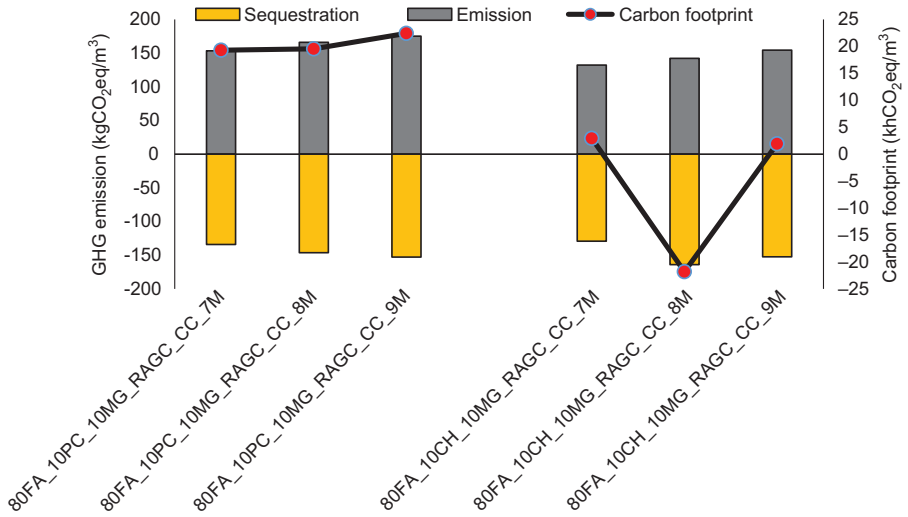

Figure 14.17 Greenhouse gas emission and carbon footprint.

sodium hydroxide concentration of 7M and the additive calcium hydroxide. As to the overall carbon footprint, while OPC-based mixtures show results around 20 $kgCO_2eq/m^3$, the mixtures based on calcium hydroxide have almost null results and the mixture based on the sodium hydroxide of 8M even shows carbon dioxide sequestration potential ($-21\ kgCO_2eq/m^3$). Other authors (Ouellet-Plamondon and Habert, 2014) reported an embodied carbon of 227 $kgCO_2eq/m^3$ for a mixture of hybrid cement-based concrete. Also Abdollahnejad et al. (2017) reported global warming potential in range of 178 and 250 $kgCO_2eq/m^3$ for one-part geopolymer foam mortars composed of FA, OPC, calcined kaolin, sodium hydroxide, and $Ca(OH)_2$. Those confirm the very good carbon footprint performance of the mixtures developed in this study.

14.3.9 Correlation between the compressive strength and carbon footprint

This stage aimed to correlate the compressive strength and carbon footprint of the mixtures. Thus, the carbon footprint of each mixture was normalized by the compressive strength of mixtures at 28 days. The amount of carbon dioxide released into the atmosphere per 1 MPa was computed by normalizing the carbon footprint to the compressive strength (Fig. 14.18). With respect to the results, regardless of the molarity, the mixture of 80FA_10CH_10 MG_RAGC_CC presented values lower than 0.2 $kgCO_2eq/m^3MPa$. The results show that the mixture based on the additive shows the lowest ratio emissions/strength. The mixture with the sodium concentration of 8M even shows a negative ratio. As to the mixtures based on OPC the worst case scenario is of 3 $kgCO_2eq/MPa$.

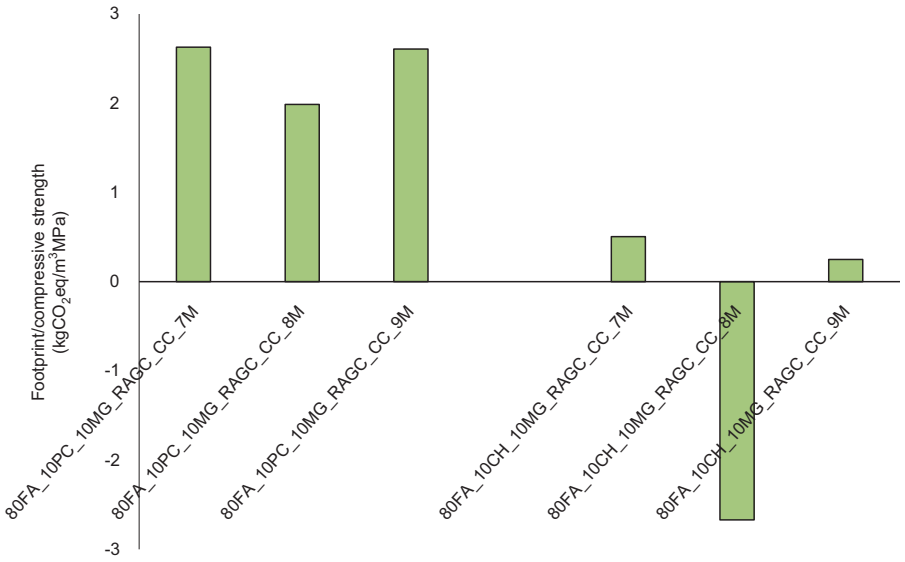

Figure 14.18 Ratio of carbon footprint to the compressive strength.

14.3.10 Cost analysis of the mixtures considering carbon tax

This stage has been assigned to assess the cost of FA alkaline-based mortars containing recycled carbonated aggregates. The cost of mixtures for one cubic meter was computed with respect to the listed prices of mixtures' ingredients in Table 14.4, which were provided by their suppliers. Moreover, two scenarios were also assumed to consider the carbon tax in the total price of each mixture, including (1) 0.0347 Euro/kg for the carbon footprint as the first scenario (Stanford Report, 2015); (2) 0.206 Euro/kg for the carbon footprint of mixtures as the second scenario (Moore and Diaz, 2015). The total costs of the mixtures are shown in Fig. 14.19 The fact that the cost of calcium hydroxide is almost three times the cost of OPC explains why for the same sodium hydroxide concentration OPC-based mixtures have a lower cost. The minimum cost is found in mixtures with the sodium hydroxide concentration of 7M being 136 Euro/m^3 for mixtures based on OPC additive and 144 Euro/m^3 for those based on calcium hydroxide. Increasing the sodium hydroxide concentration to 9M leads to a cost of 144 Euro/m^3 for mixtures based on OPC and of 152 Euro/m^3 for mixtures using calcium hydroxide additive. When a carbon tax with the value

Table 14.4 Costs of the materials (Euro/kg)

Recycled aggregates	MG	CH	Fly ash	Water	PC	SH
0.047	0.009	0.283	0.03	0.01	0.1	0.85

CH, calcium hydroxide; *FA*, fly ash; *MG*, waste glass; *PC*, Portland cement; *SH*, sodium hydroxide.

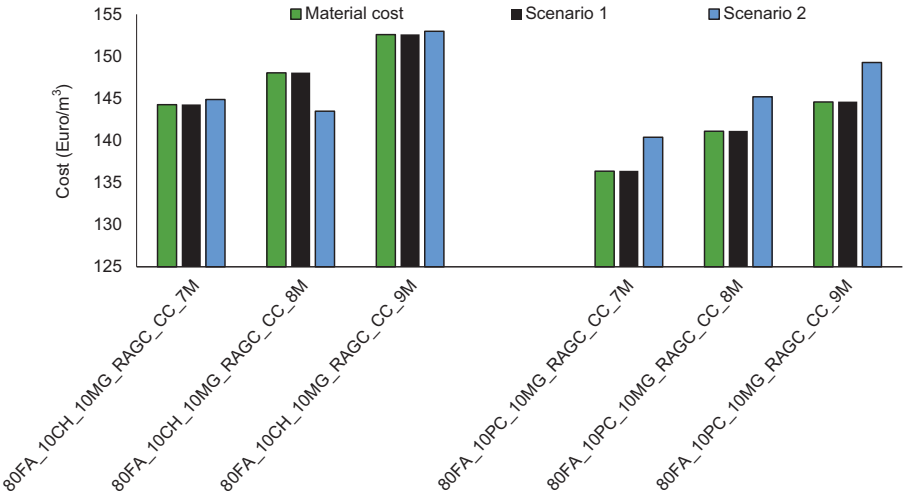

Figure 14.19 Cost of the mixtures.

of 0.0347 Euro/kg is considered (scenario 1), the results follow the same previous trend meaning that such carbon value is too low to lead to visible changes. As to the scenario 2 with a higher carbon tax it leads to a minor increase of around 4% in the cost of mixtures using the OPC additive. For this scenario mixtures based on OPC additive and a sodium hydroxide concentration of at least 8M would have a cost similar to calcium hydroxide-based mixtures. However, since the mixtures with the calcium hydroxide additive have a much lower carbon footprint, the mixtures with the sodium hydroxide concentration of 7 and 9M show no cost increase while the mixture with the sodium hydroxide concentration of 8M shows a minor reduction which is explained by its carbon sequestration capacity.

14.4 Conclusions

The mixtures with calcium hydroxide and sodium hydroxide concentration of 8M lead to the highest compressive strength (10 MPa) which is high enough for the production of masonry blocks. The results show that the replacement of Portland cement by calcium hydroxide is associated with an increase in the compressive strength due to the formation of a higher amount of CSH gel. The maximum flexural strength is 3.5 MPa. Significant correlations between the flexural strength and the compressive strength were noticed. The mixtures show low water absorption by immersion (9%), as well as by capillarity (1.4 kg/m^2 $H^{0.5}$), and it is possible that the accelerated carbonation curing has been responsible for the coarser capillary network. The results of the modulus of elasticity show that increasing the sodium hydroxide molarity increased the stiffness of the mixtures. Also a significant correlation between elastic modulus and compressive strength was found in the mixture based on OPC. The results of

drying shrinkage are in line with the results of the capillary water absorption and of elastic modulus. A maximum CO_2 sequestration (164 $kgCO_2eq/m^3$) is noticed for the mixture with a sodium concentration of 8M based on the additive calcium hydroxide. The overall carbon footprint results show that while mixtures with OPC additive show results around 20 $kgCO_2eq/m^3$, the mixtures based on calcium hydroxide have almost null results and the mixture based on the sodium hydroxide of 8M even shows carbon dioxide sequestration potential (−21 $kgCO_2eq/m^3$). For the same sodium hydroxide concentration, OPC-based mixtures have a lower cost. The minimum cost is of 136 $Euro/m^3$ for the sodium hydroxide concentration of 7M. The carbon tax of 0.0347 Euro/kg shows no influence on the cost of the mixtures while the carbon tax of 0.206 Euro/kg shows an increase in the cost eco-efficiency of mixtures with the additive calcium hydroxide as well as a minor reduction in the cost of mixture with carbon sequestration capacity.

Acknowledgment

The authors would like to acknowledge the financial support of the Foundation for Science and Technology (FCT) in the frame of project IF/00706/2014-UM.2.15.

References

Abdollahnejad, Z., Miraldo, S., Pacheco-Torgal, F., Barroso Aguiar, J., 2017. Cost-efficient one-part alkali-activated mortars with low global warming potential for floor heating systems applications. European Journal of Environmental and Civil Engineering 21, 412−429.

Alonso, S., Palomo, A., 2001a. − Alkaline Activation of metakaolin and calcium hydroxide mixtures: influence of temperature, activator concentration and solids ratio. Materials Letters 47, 55−62.

Alonso, S., Palomo, A., 2001b. − Calorimetric study of alkaline activation of calcium hydroxide-metakaolin solid mixtures. Cement and Concrete Research 31, 25−30.

ASTM C618-15, 2015. Standard Specification for Coal Fly Ash and Raw or Calcined Natural Pozzolan for Use in Concrete. ASTM International, West Conshohocken, PA. www.astm.org.

ASTM C109/C109M-16a, 2016. Standard Test Method for Compressive Strength of Hydraulic Cement Mortars (Using 2-in. Or [50-mm] Cube Specimens). ASTM International, West Conshohocken, PA. www.astm.org.

Atis, C.D., Görür, E.B., Karahan, O., Bilim, C., Ilkentapar, S., Luga, E., 2015. Very high strength (120 MPa) class F fly ash geopolymer mortar activated at different NaOH amount, heat curing temperature and heat curing duration. Construction and Building Materials 96, 673−678.

Bernal, S., Rodríguez, E., Kirchheim, A., Provis, J., 2016. Management and valorisation of wastes through use in producing alkali-activated. Cement materials. Journal of Chemical Technology & Biotechnology. https://doi.org/10.1002/jctb.4927.

El-Hassan, H., Shao, Y., 2015. Early carbonation curing of concrete masonry units with Portland limestone cement. Cement and Concrete Composites 62, 168−177.

El-Hassan, H., Shao, Y., 2014. Carbon storage through concrete block carbonation. Journal of Clean Energy Technology 2, 287−291.

Garcia-Lodeiro, I., Donatello, S., Fernandez-Jimenez, A., Palomo, A., 2016. Hydration of hybrid alkaline cement containing a very large proportion of fly ash:A Descriptive Model. Materials 9, 605.

Gorhan, G., Kurklu, G., 2014. The influence of the NaOH solution on the properties of the fly ash-based geopolymer mortar cured at different temperatures. Composites Part B: Engineering 58, 371−377.

Hanjitsuwan, S., Hunpratub, S., Thongbai, P., Maensiri, S., Sata, V., Chindaprasirt, P., 2014. Effects of NaOH concentrations on physical and electrical properties of high calcium fly ash geopolymer paste. Cement and Concrete Composites 45, 9−14.

Jang, J.G., Lee, H.K., 2016. Microstructural densification and CO_2 uptake promoted by the carbonation curing of belite-rich Portland cement. Cement and Concrete Research 82, 50−57.

Martinez-Lopez, R., Escalante-Garcia, J.I., 2016. Alkali-activated composite binders of waste silica soda lime glass and blast furnace slag: Strength as a function of the composition. Construction and Building Materials 119, 119−129.

Moore, F., Diaz, D., 2015. Temperature impacts on economic growth warrant stringent mitigation policy. Nature Climate Change 5, 127−131.

Ouellet-Plamondon, C., Habert, G., 2014. Life cycle analysis (LCA) of alkali-activated cements and concretes. In: Pacheco-Torgal, F., Labrincha, J., Palomo, A., Leonelli, C., Chindaprasirt, P. (Eds.), Handbook of Alkali-activated Cements, Mortars and Concretes. WoodHead Publishing-Elsevier, Cambridge, pp. 663−686.

Pacheco-Torgal, F., Abdollahnejad, Z., Miraldo, S., Kheradmand, M., 2016. Alkali-activated cement-based binders (AACB) as durable and cost competitive low CO_2 binders: some shortcomings that need to be addressed. In: Nazari, Sanjayan (Eds.), Handbook of Low Carbon Concrete. Elsevier Science and Tech, Waltham, US, pp. 1−15.

Provis, J.L., 2014. Geopolymers and other alkali activated materials: why, how, and what ? Materials and Structures 47, 11−25. https://doi.org/10.1617/s11527-013-0211-5.

Rattanasak, U., Chindaprasirt, P., 2009. Influence of NaOH solution on the synthesis of fly ash geopolymer. Minerals Engineering 22, 1073−1078.

Sata, V., Wongsa, A., Chindaprasirt, P., 2013. Properties of pervious geopolymer concrete using recycled aggregates. Construction and Building Materials 42, 33−39.

Šavija, B., Luković, M., 2016. Carbonation of cement paste: understanding, challenges, and opportunities. Construction and Building Materials 117, 285−301.

Stanford Report, 2015. Estimated Social Cost of Climate Change Not Accurate, Stanford Scientists Say. Retrieved from: http://news.stanford.edu/news/2015/january/emissions-social-costs-011215.

Wang, W.-C., Chen, B.-T., Wang, H.-Y., Chou, H.-C., 2016. A study of the engineering properties of alkali-activated waste glass material (AAWGM). Construction and Building Materials 112, 962−969.